Peristaltic Motion of a non-Newtonian Nanofluid in an Asymmetric Channel

Fahad Munir Abbasi[a], Tasawar Hayat[a,b], Bashir Ahmad[b], and Guo-Qian Chen[b,c]

[a] Department of Mathematics, Quaid-I-Azam University 45320, Islamabad 44000, Pakistan
[b] Nonlinear Analysis and Applied Mathematics (NAAM) Research Group, Faculty of Science, King Abdulaziz University, Jeddah 21589, Saudi Arabia
[c] College of Engineering, Peking University, Beijing, China

Reprint requests to F. M. A.; E-mail: abbasisarkar@gmail.com

Z. Naturforsch. **69a**, 451 – 461 (2014) / DOI: 10.5560/ZNA.2014-0041
Received December 23, 2013 / revised April 12, 2014 / published online July 30, 2014

The peristaltic transport of a Carreau–Yasuda fluid in an asymmetric channel is studied. Problem formulation is given in the presence of nanoparticles and contributions of Brownian motion and thermophoresis are taken into account. Lubrication approach is employed. The resulting nonlinear system of equations is solved numerically, and the effects of sundry parameters on the velocity, temperature, and concentration are analyzed. Heat and mass transfer rates are computed and examined. The results show that the impact of the non-Newtonian parameters on flow quantities get reversed when we move from shear thinning to shear thickening fluids. The temperature of the nanofluid in presence of Brownian motion increases, furthermore the influence of Brownian motion parameter on temperature and concentration distributions is opposite.

Key words: Nanoparticles; Carreau–Yasuda Fluid; Peristaltic Motion; Mathematical Modelling.

1. Introduction

It is well admitted fact that common fluids (e. g. water, oil, ethylene, glycol etc.) are poor conductors of heat owing to their low thermal conductivity. This brings to light a need of methods to enhance the thermal conductivity of fluids. Change in flow geometry, use of various type of boundary conditions, enhancement of thermal conductivity are some techniques used by several investigators just to facilitate the heat transfer in fluids during the past few decades. Suspension of micro sized solid particles was also used to enhance the thermal conductivity. This technique proved less fruitful because micro meter size turned out to be too large as the solute provided additional resistance to the flow and the ability of these particles to settle out of the suspension. The use of particles with size below 50 nanometer (nanoparticles) for the suspension has been recognized very useful for enhancement of thermal conductivity of the fluids. The research on the nanofluids are about understanding their characteristics so that they can be utilized where straight heat transfer enhancement is paramount as in many industrial processes which include microelectronics, transportation, nuclear reactors, food and biomedicine, solid state lighting and manufacturing. Undoubtedly the nanofluids remarkably enhance the thermal conductivity of a conventional liquid which is beyond the description of any available theory. Such fluids are very stable and have no extra issues of erosion, sedimentation, additional pressure drop etc. This is because of the tiny size and low volume fraction of nanoelements required for the thermal conductivity enhancement. The literature now on this topic is quite sizeable (see some recent articles [1 – 10] amongst the others).

Mechanical analysis of the non-Newtonian fluids gained much importance due to their occurrence in nature and industry. However a single constitutive equation of non-Newtonian fluid is inadequate to predict the diverse properties of all such fluids. As expected these fluids differ in their characteristics. Therefore many models of non-Newtonian fluids are proposed. The Carreau–Yasuda (CY) fluid is one amongst these models. Main advantage of this model over the so called power law model is that the Carreau–Yasuda model contains five parameters to explain the fluid rheology when compared with three constants of the power law model. The shear thinning and shear thickening effects

can be predicted by the CY model with great accuracy. In its limiting case it can predict the results of Carreau as well as the Newtonian fluid models. Gijsen et al. [11, 12] investigated the non-Newtonian properties of blood in large arteries. In these studies the authors compared the experimental results with the numerical data using the CY model. A good agreement between the experimental and numerical results is noticed. Andrade et al. [13] computed skin friction for turbulent flow in pipes using the CY model.

Peristalsis is a well-known phenomenon of fluid transport in many physiological and industrial processes. Transport of food through oesophagus, chyme movement in intestine, urine transport from kidney to bladder, bile movement from gallbladder to duodenum, spermatozoa transport in male reproductive tract are some physiological processes comprising peristalsis. In industry, peristalsis is used for transportation of corrosive/sensitive fluids, in roller/finger pumps, in heart-lung and dialysis machines. In this mechanism waves of area contraction and relaxation propagate along the walls of channel/tube containing the fluid. These waves propel the fluid in the direction of propagation. Further, the concept of heat transfer is significant in the analysis of tissues, hemodialysis, and oxygenation. The recent progress in the application of heat (hyperthermia), radiation (laser therapy), and coldness (cryosurgery), as means to destroy undesirable tissues including cancer have stimulated much interest in mathematical modelling for properties of tissue. Filtration of blood in kidneys, exchange of gases in lungs, food absorption in intestines during intestinal peristalsis, absorption of water and salts by the roots of plants, exchange of gases between the atmosphere and plant leaves, ores separation, metal purification, nuclear reactors etc. are some processes involving mass transfer. Through such motivations the peristaltic transport with heat/mass transfer was analyzed in the studies [14 – 25].

Previous literature indicates that peristalsis of non-Newtonian fluids with nanoparticles is not focused much. The purpose here is to venture further in this regime. The fluids are now known as non-Newtonian in numerous physiological and industrial processes. The fluids in the presence of nanoparticles are important especially in hyperthermia, cancer therapy, tumor analysis, optical switches building construction, geothermal, oil recovery, and many others. It is also noticed that the intra-uterine fluid flow in peristalsis due to myometrial contractions occur in both symmetric and asymmetric directions. The characterization of non-pregnant woman uterine contractions is very complicated as they are composed of variable amplitudes, a range of frequencies, and different wavelengths. The width of the sagittal cross-section of the uterine cavity increases towards the fundus, and the cavity is not fully occluded during the contraction. With all such in mind, the present investigation models the problem of peristaltic transport of a CY-nanofluid in an asymmetric channel. To our knowledge such analysis is not presented before. The relevant flow model is first non-dimensionalized and then simplified subject to long wavelength and low Reynolds number approximations. The involved system even after such simplification is nonlinear. The resulting nonlinear problem is numerically solved for the flow quantities of interest. Attention is mainly fo-

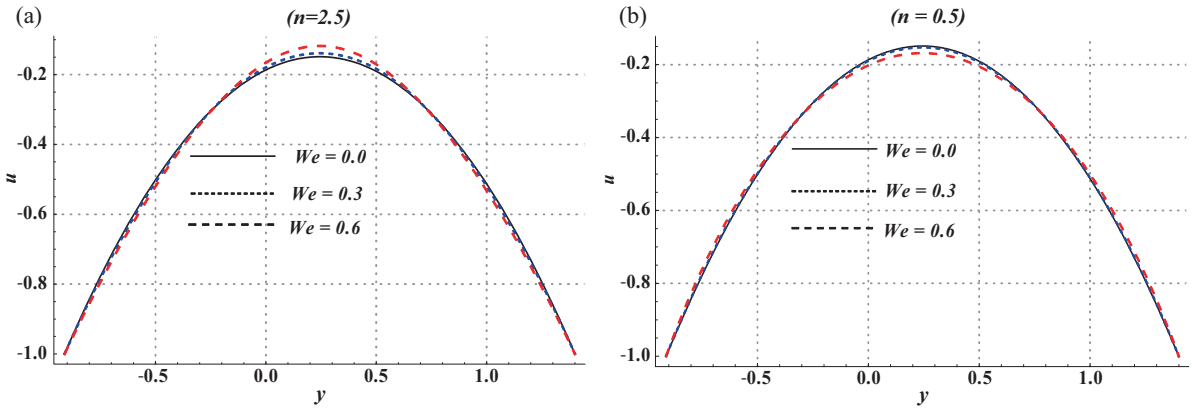

Fig. 1 (colour online). Velocity profiles for the variation in Weissenberg number We when $a = 2$, Br $= 0.3$, $x = 0.0$, $a_2 = 0.4$, $b_2 = 0.3$, $\gamma = \pi/4$, $d = 0.7$, $\rho = 0.7$, Pr $= 0.5$, $N_t = 0.5$, $N_b = 0.5$, and $\beta = 0.1$.

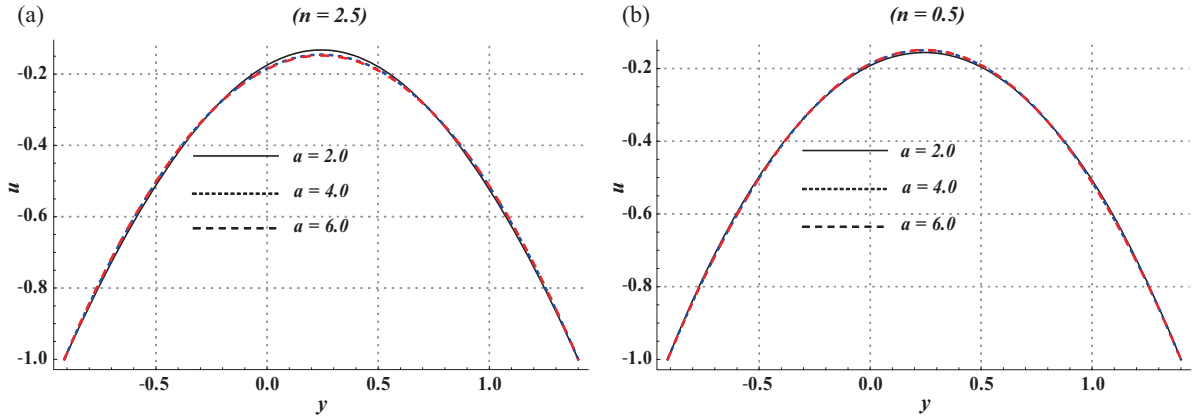

Fig. 2 (colour online). Velocity profiles for the variation in non-Newtonian parameter a when We $= 0.4$, Br $= 0.3$, $x = 0.0$, $a_2 = 0.4$, $b_2 = 0.3$, $\gamma = \pi/4$, $d = 0.7$, $\eta = 0.7$, Pr $= 0.5$, $N_t = 0.5$, $N_b = 0.5$, and $\beta = 0.1$.

cused to the salient features of rheological parameters, Brownian motion, and thermophoresis. Numerical values of heat and mass transfer rates are presented and analyzed in tabular form. It is hoped that the present research will be a stimulus for several further fundamental investigations on the topic in future.

2. Problem Formulation

We consider the flow of an incompressible Carreau–Yasuda fluid containing nanoparticles in a two-dimensional asymmetric channel of width $\bar{d}_1 + \bar{d}_2$. Flow in the channel is generated due to sinusoidal wave trains propagating along the channel walls with constant wave speed c. The geometry of wall surfaces is defined as

$$\begin{aligned} \bar{H}_1(\bar{X},\bar{t}) &= \bar{d}_1 + \bar{\varepsilon}_1 \quad \text{(upper wall) and} \\ \bar{H}_2(\bar{X},\bar{t}) &= -\left(\bar{d}_2 + \bar{\varepsilon}_2\right) \quad \text{(lower wall)}, \end{aligned} \tag{1}$$

where $\bar{\varepsilon}_1$ and $\bar{\varepsilon}_2$ are the disturbances produced due to propagation of peristaltic waves along the upper and lower walls, respectively. These disturbances are of the forms

$$\begin{aligned} \bar{\varepsilon}_1 &= \bar{b}_1 \cos\left(\frac{2\pi}{\lambda}\left(\bar{X} - c\bar{t}\right)\right), \\ \bar{\varepsilon}_2 &= \bar{b}_2 \cos\left(\frac{2\pi}{\lambda}\left(\bar{X} - c\bar{t}\right) + \gamma\right), \end{aligned} \tag{2}$$

in which $\bar{b}_1$, $\bar{b}_2$ are the amplitudes of the waves, γ $(0 \le \gamma \le \pi)$ is the phase difference, $\bar{t}$ is the time, λ is the wavelength, and $\bar{X}$ and $\bar{Y}$ are the rectangular coordinates with $\bar{X}$ measured along the channel length and $\bar{Y}$ normal to $\bar{X}$. It is important to mention that $\gamma = 0$ and $\gamma = \pi$ correspond to the cases where the channel is symmetric with waves out of phase and waves in phase, respectively. Moreover $\bar{d}_1$, $\bar{d}_2$, $\bar{b}_1$, $\bar{b}_2$, and γ satisfy the condition

$$\bar{d}_1^2 + \bar{d}_2^2 + 2\bar{b}_1\bar{b}_2\cos\gamma \le \left(\bar{d}_1 + \bar{d}_2\right).$$

The velocity field for such flow is taken to be $\mathbf{V} = \left[\bar{U}\left(\bar{X},\bar{Y},\bar{t}\right),\bar{V}\left(\bar{X},\bar{Y}\bar{t}\right),\bar{t}\right]$. The conservation of mass, momentum, energy, and concentration equations for two-dimensional incompressible flow are

$$\frac{\partial \bar{U}}{\partial \bar{X}} + \frac{\partial \bar{V}}{\partial \bar{Y}} = 0, \tag{3}$$

$$\rho_f\left(\frac{\partial}{\partial \bar{t}} + \bar{U}\frac{\partial}{\partial \bar{X}} + \bar{V}\frac{\partial}{\partial \bar{Y}}\right)\bar{U} = -\frac{\partial \bar{P}}{\partial \bar{X}} + \frac{\partial \bar{S}_{\bar{X}\bar{X}}}{\partial \bar{X}} + \frac{\partial \bar{S}_{\bar{X}\bar{Y}}}{\partial \bar{Y}}, \tag{4}$$

$$\rho_f\left(\frac{\partial}{\partial \bar{t}} + \bar{U}\frac{\partial}{\partial \bar{X}} + \bar{V}\frac{\partial}{\partial \bar{Y}}\right)\bar{V} = -\frac{\partial \bar{P}}{\partial \bar{Y}} + \frac{\partial \bar{S}_{\bar{Y}\bar{X}}}{\partial \bar{X}} + \frac{\partial \bar{S}_{\bar{Y}\bar{Y}}}{\partial \bar{Y}}, \tag{5}$$

$$\rho_f C_f\left(\frac{\partial}{\partial \bar{t}} + \bar{U}\frac{\partial}{\partial \bar{X}} + \bar{V}\frac{\partial}{\partial \bar{Y}}\right)T = K\left[\frac{\partial^2 T}{\partial \bar{X}^2} + \frac{\partial^2 T}{\partial \bar{Y}^2}\right] + \bar{S}\cdot\mathbf{L} + \tau\rho_f C_f\left[D_B\left(\frac{\partial C}{\partial \bar{X}}\frac{\partial T}{\partial \bar{X}} + \frac{\partial C}{\partial \bar{Y}}\frac{\partial T}{\partial \bar{Y}}\right) + \frac{D_T}{T_m}\left(\frac{\partial^2 T}{\partial \bar{X}^2} + \frac{\partial^2 T}{\partial \bar{Y}^2}\right)\right], \tag{6}$$

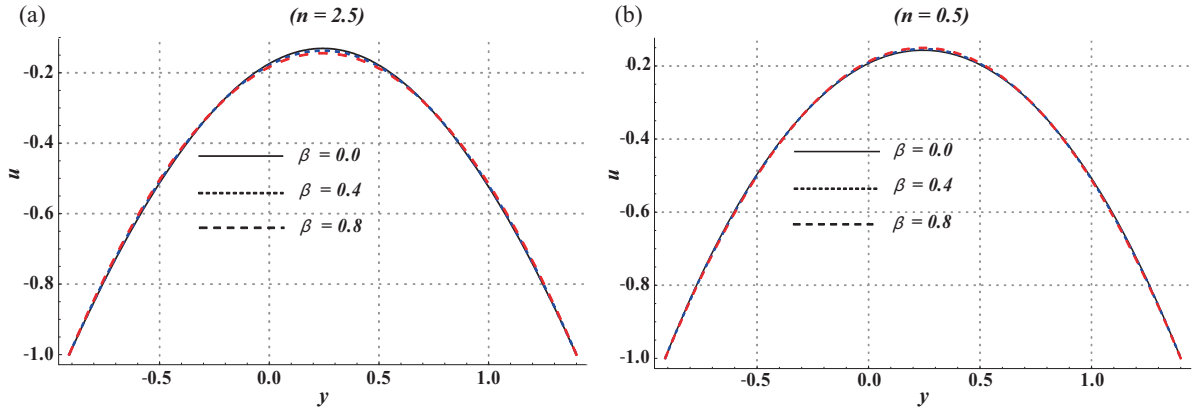

Fig. 3 (colour online). Velocity profiles for the variation in viscosity parameter β when $a = 2$, Br $= 0.3$, $x = 0.0$, $a_2 = 0.4$, $b_2 = 0.3$, $\gamma = \pi/4$, $d = 0.7$, $\eta = 0.7$, Pr $= 0.5$, $N_t = 0.5$, $N_b = 0.5$, and $a = 2.0$.

$$\left[\frac{\partial}{\partial \bar{t}} + \bar{U}\frac{\partial}{\partial \bar{X}} + \bar{V}\frac{\partial}{\partial \bar{Y}}\right] C = D_B\left[\frac{\partial^2 C}{\partial \bar{X}^2} + \frac{\partial^2 C}{\partial \bar{Y}^2}\right] + \frac{D_T}{T_m}\left[\frac{\partial^2 T}{\partial \bar{X}^2} + \frac{\partial^2 T}{\partial \bar{Y}^2}\right]. \tag{7}$$

In these equations, P is the pressure, ρ_f the density of the base fluid, $\bar{S}_{ij}$ are the components of the extra stress tensor, T is the fluid temperature, C the concentration, $\bar{S}\cdot\mathbf{L}$ the viscous dissipation term, $\mathbf{L}$ the gradient of velocity, C_f the specific heat of the fluid, K the thermal conductivity of the fluid, D_B the mass diffusivity, K_T the thermal diffusion ratio, C_S the concentration susceptibility, T_m the fluid mean temperature, and $\tau = \frac{(\rho C)_p}{(\rho C)_f}$, where $(\rho C)_p$ is the effective heat capacity of the nanoparticles. In order to transform our problem from the fixed frame (laboratory frame) to a frame of reference moving with the wave speed c (wave frame), we use the following transformations:

$$\bar{x} = \bar{X} - c\bar{t}\,,\quad \bar{y} = \bar{Y}\,,\quad \bar{u} = \bar{U} - c\,,$$
$$\bar{v} = \bar{V}\,,\quad \bar{p}(\bar{x},\bar{y}) = \bar{P}(\bar{X},\bar{Y},\bar{t})\,, \tag{8}$$

in which $\bar{u}$, $\bar{v}$, and $\bar{p}$ are the velocity components and pressure in the wave frame $(\bar{x},\bar{y})$. In the wave frame, (3)–(7) become

$$\frac{\partial \bar{u}}{\partial \bar{x}} + \frac{\partial \bar{v}}{\partial \bar{y}} = 0\,, \tag{9}$$

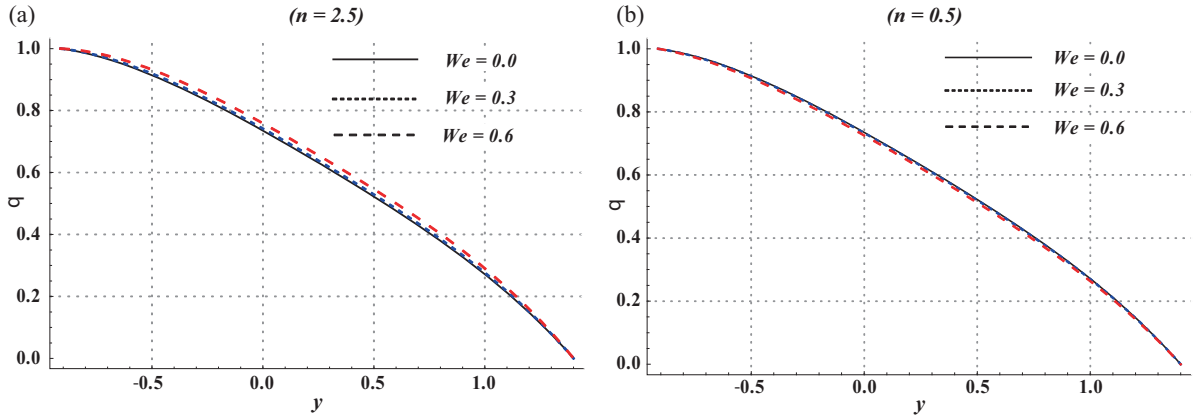

Fig. 4 (colour online). Variation in temperature via Weissenberg number We when $a = 2$, Br $= 0.3$, $x = 0.0$, $a_2 = 0.4$, $b_2 = 0.3$, $\gamma = \pi/4$, $d = 0.7$, $\eta = 0.7$, $N_t = 0.5$, $N_b = 0.5$, and $\beta = 0.1$.

$$\rho_{\mathrm{f}}\left((\bar{u}+c)\frac{\partial}{\partial\bar{x}}+\bar{v}\frac{\partial}{\partial\bar{y}}\right)(\bar{u}+c)= -\frac{\partial\bar{p}}{\partial\bar{x}}+\frac{\partial\bar{s}_{\bar{x}\bar{x}}}{\partial\bar{x}}+\frac{\partial\bar{s}_{\bar{x}\bar{y}}}{\partial\bar{y}}, \tag{10}$$

$$\rho_{\mathrm{f}}\left((\bar{u}+c)\frac{\partial}{\partial\bar{x}}+\bar{v}\frac{\partial}{\partial\bar{y}}\right)\bar{v}=-\frac{\partial\bar{p}}{\partial\bar{y}}+\frac{\partial\bar{s}_{\bar{y}\bar{x}}}{\partial\bar{x}}+\frac{\partial\bar{S}_{\bar{y}\bar{y}}}{\partial\bar{y}}, \tag{11}$$

$$\rho_{\mathrm{f}}C_{\mathrm{f}}\left((\bar{u}+c)\frac{\partial}{\partial\bar{x}}+\bar{v}\frac{\partial}{\partial\bar{y}}\right)T=K\left[\frac{\partial^2T}{\partial\bar{x}^2}+\frac{\partial^2T}{\partial\bar{x}^2}\right] +\bar{s}\cdot\bar{\mathbf{L}}+\tau\rho_{\mathrm{f}}C_{\mathrm{f}}\left[D_B\left(\frac{\partial C}{\partial\bar{x}}\frac{\partial T}{\partial\bar{x}}+\frac{\partial C}{\partial\bar{y}}\frac{\partial T}{\partial\bar{y}}\right)+\frac{D_{\mathrm{T}}}{T_{\mathrm{m}}}\left(\frac{\partial^2T}{\partial\bar{x}^2}+\frac{\partial^2T}{\partial\bar{y}^2}\right)\right], \tag{12}$$

$$\left[(\bar{u}+c)\frac{\partial}{\partial\bar{x}}+\bar{v}\frac{\partial}{\partial\bar{y}}\right]C=D_B\left[\frac{\partial^2C}{\partial\bar{x}^2}+\frac{\partial^2C}{\partial\bar{y}^2}\right]+\frac{D_{\mathrm{T}}}{T_{\mathrm{m}}}\left[\frac{\partial^2T}{\partial\bar{x}^2}+\frac{\partial^2T}{\partial\bar{y}^2}\right]. \tag{13}$$

Here $\bar{s}_{ij}$ are components of the extra stress tensor in the wave frame, $\bar{\mathbf{L}}$ is the velocity gradient, and $\bar{s}\cdot\bar{\mathbf{L}}$ the viscous dissipation term in wave frame. Considering the dimensionless quantities

$$x=\frac{\bar{x}}{\lambda},\ y=\frac{\bar{y}}{\bar{d}_1},\ u=\frac{\bar{u}}{c},\ v=\frac{\bar{v}}{c\delta},\ \delta=\frac{\bar{d}_1}{\lambda},$$
$$h_1=\frac{\bar{H}_1}{\bar{d}_1},\ h_2=\frac{\bar{H}_2}{\bar{d}_1},\ d=\frac{\bar{d}_2}{\bar{d}_1},\ a_1=\frac{\bar{b}_1}{d_1},\ b=\frac{\bar{b}_2}{d_1},$$
$$p=\frac{d_1^2\bar{p}}{c\lambda\mu},\ \theta=\frac{T-T_0}{T_1-T_0},\ \phi=\frac{C-C_0}{C_1-C_0},\ \mathrm{Re}=\frac{\rho_{\mathrm{f}}c\bar{d}_1}{\mu},$$
$$S_{xy}=\frac{d_1\bar{S}_{\bar{x}\bar{y}}}{\mu_0c},\ t=\frac{c\bar{t}}{\lambda},\ \mathrm{Br}=\mathrm{Pr}E,\ E=\frac{c^2}{C_{\mathrm{f}}(T_1-T_0)},$$
$$\mathrm{Pr}=\frac{\mu C_{\mathrm{f}}}{K},\ N_{\mathrm{b}}=\frac{\tau D_B(C_1-C_0)}{\upsilon},\ N_{\mathrm{t}}=\frac{\tau D_{\mathrm{T}}(T_1-T_0)}{\upsilon T_{\mathrm{m}}},$$
$$u=\frac{\partial\psi}{\partial y},\ v=-\frac{\partial\psi}{\partial x}, \tag{14}$$

and applying the long wavelength and low Reynolds number approximations [16 – 19], we have

$$p_x=\frac{\partial s_{xy}}{\partial y}, \tag{15}$$

$$p_y=0, \tag{16}$$

$$\theta_{yy}+\mathrm{Br}\Phi+\mathrm{Pr}N_{\mathrm{b}}\phi_y\theta_y+\mathrm{Pr}N_{\mathrm{t}}\left(\theta_y\right)^2=0, \tag{17}$$

$$\phi_{yy}+\left(\frac{N_{\mathrm{t}}}{N_{\mathrm{b}}}\right)\theta_{yy}=0, \tag{18}$$

where the continuity equation is identically satisfied, x and y are the dimensionless coordinate axes, u, v, h_1, h_2, d, a_1, b are the x-component of velocity, y-component of velocity, dimensionless upper wall, dimensionless lower wall, channel width ratio, dimensionless amplitude of the wave at upper and lower walls, respectively. Also here Re denotes the Reynolds number, s_{xy} the dimensionless component of extra stress tensor, ψ the stream function, Br the Brinkman number, E the Eckret number, Pr the Prandtl number, δ the wave number, Φ is the dimensionless viscous dissipation term, ϕ dimensionless concentration, θ the dimensionless temperature, T_0, C_0 the temperature and concentration at the upper wall, T_1, C_1 the temperature and concentration at the lower wall, N_{b} the Brownian motion parameter, and N_{t} the thermophoresis parameter. Moreover the compatibility equation can be obtained through cross differentiation of (15) and (16). We write

$$\frac{\partial^2}{\partial y^2}s_{xy}=0. \tag{19}$$

The extra stress tensor for the Carreau–Yasuda fluid is given as [11 – 13]

$$\bar{S}=\mu\left(\gamma'\right)A_1, \tag{20}$$

where A_1 is the first Rivlin–Erickson tensor and $\mu(\gamma')$ is the apparent viscosity defined by

$$\mu\left(\gamma'\right)=\mu_\infty+(\mu_0-\mu_\infty)\left[1+\left(\Gamma\gamma'\right)^a\right]^{\frac{n-1}{a}}$$
$$\text{with}\ \ \gamma'=\sqrt{2\mathrm{tr}(D^2)}\ \ \text{and}$$
$$D=\frac{1}{2}\left[\mathrm{grad}\mathbf{V}+(\mathrm{grad}\mathbf{V})^{\mathrm{T}}\right]=\frac{1}{2}A_1. \tag{21}$$

Here μ_0 is the zero shear-rate viscosity, μ_∞ the infinite shear-rate viscosity, grad$\mathbf{V}$ denotes the gradient of velocity, n the dimensionless power law index, Γ and a the dimensional and dimensionless non-Newtonian parameters, respectively. This fluid model has the ability to depict the flow of a Newtonian fluid with viscosities μ_0 and μ_∞ at the lower and upper ends of shear rate range. The non-Newtonian parameters Γ and a control the transition between the two extremes. This model predicts the results of shear thinning fluid for $n<1$ and shear thickening fluid for $n>1$. For $n=1$ the results of Newtonian fluid are obtained. The results for the Carreau fluid model can also be retained by substituting $a=2$. The dimensionless form of the extra stress tensor under the low Reynolds number and long wavelength approximation becomes

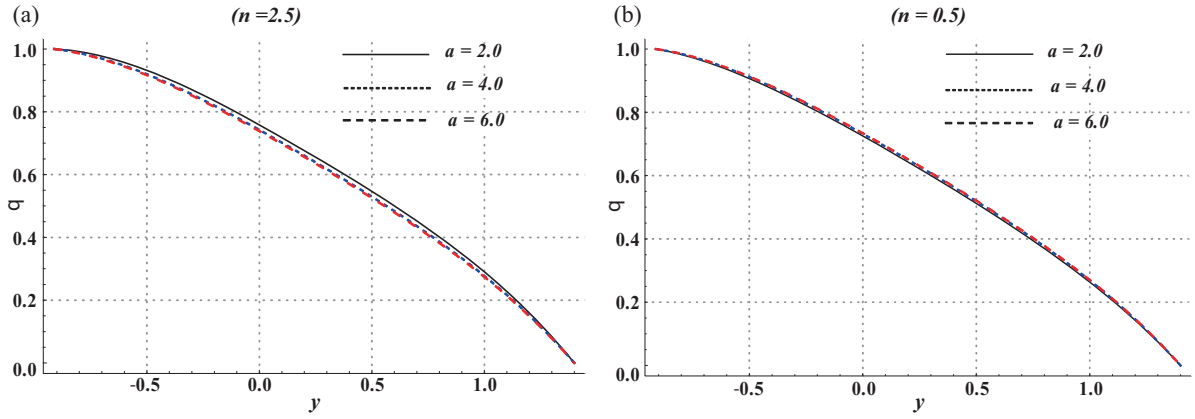

Fig. 5 (colour online). Variation in temperature via non-Newtonian parameter a when We $= 0.6$, Br $= 0.3$, $x = 0.0$, $a_2 = 0.4$, $b_2 = 0.3$, $\gamma = \pi/4$, $d = 0.7$, $\eta = 0.7$, Pr $= 0.5$, $N_t = 0.5$, $N_b = 0.5$, and $\beta = 0.1$.

$$s_{xy} = s_{yx} = \left[1+\frac{(1-\beta)(n-1)\mathrm{We}^a}{a}\left(\psi_{yy}\right)^a\right]\psi_{yy}. \quad (22)$$

Here $\beta = \frac{\mu_\infty}{\mu_0}$ is the viscosity ratio parameter and We $= \frac{\Gamma c}{d_1}$ the Weissenberg number.

3. Flow Rate and Boundary Conditions

Taking $\bar{H}_{1,2}$ as functions of $\bar{X}$ and $\bar{t}$, the dimensionless volume flow rate in laboratory frame is

$$Q = \int_{\bar{H}_2}^{\bar{H}_1} \bar{U}\left(\bar{X},\bar{Y},\bar{t}\right)\mathrm{d}\bar{Y}$$

and in the wave frame, we have

$$q = \int_{\bar{h}_2}^{\bar{h}_1} \bar{u}(x,y)\,\mathrm{d}\bar{y},$$

in which h is a function of x alone. From these relations, we can write

$$Q = q + c\bar{h}_1(x) - c\bar{h}_2(x).$$

The time averaged flow over a period T_f is given by

$$\bar{Q} = \frac{1}{\bar{T}}\int_0^{T_f} Q\,\mathrm{d}t,$$

which implies that

$$\bar{Q} = q + c\bar{d}_1 + c\bar{d}_2.$$

Defining η and F as the dimensionless mean flows in laboratory and wave frames by

$$\eta = \frac{\bar{Q}}{c\bar{d}_1}, \quad F = \frac{q}{c\bar{d}_1}, \quad (23)$$

we have

$$\eta = F + 1 + d, \quad (24)$$

where

$$F = \int_{h_2}^{h_1}\frac{\partial\psi}{\partial y}\,\mathrm{d}y. \quad (25)$$

The dimensionless boundary conditions are

$$\begin{aligned}&\psi = F/2, \ \frac{\partial\psi}{\partial y} = -1, \ \theta = 0, \ \phi = 0 \ \text{ at } y = h_1,\\ &\psi = -F/2, \ \frac{\partial\psi}{\partial y} = -1, \ \theta = 1, \ \phi = 1 \ \text{ at } y = h_2.\end{aligned} \quad (26)$$

Substituting the value of s_{xy} from (22) into (17)–(19), we get

$$\begin{aligned}&\theta_{yy} + \mathrm{Br}\left[1+\frac{(1-\beta)(n-1)\mathrm{We}^a}{a}\left(\psi_{yy}\right)^a\right]\psi_{yy}^2\\ &+\mathrm{Pr}N_b\phi_y\theta_y + \mathrm{Pr}N_t\left(\theta_y\right)^2 = 0,\end{aligned} \quad (27)$$

$$\phi_{yy} + \left(\frac{N_t}{N_b}\right)\theta_{yy} = 0, \quad (28)$$

$$\frac{\partial^2}{\partial y^2}\left[1+\frac{(1-\beta)(n-1)\mathrm{We}^a}{a}\left(\psi_{yy}\right)^a\right]\psi_{yy} = 0. \quad (29)$$

The nonlinear equations (27)–(29) subject to boundary conditions (26) are difficult to solve for closed form solutions. Hence we compute the numerical solution through built-in NDSolve command of Mathematica®. We have taken the step size equal to 0.01 for variation in both x and y. The obtained numerical results are analyzed graphically in the next section.

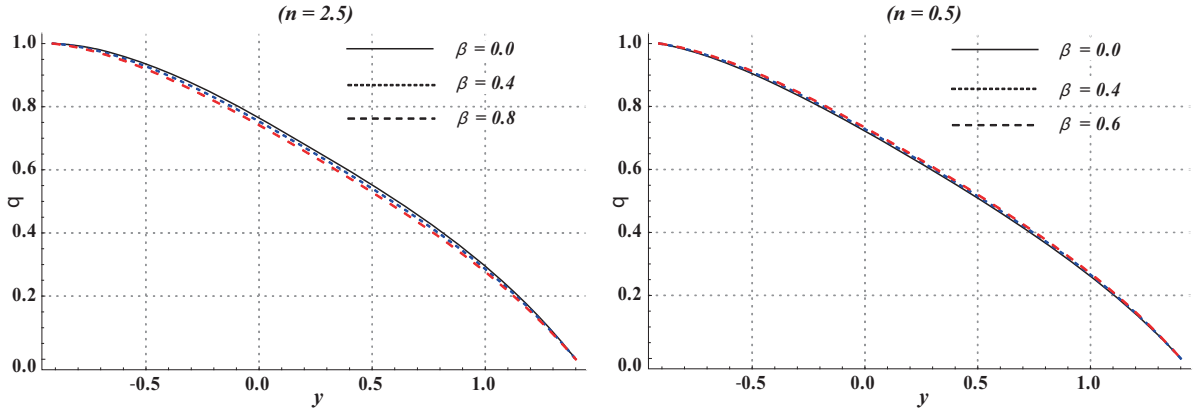

Fig. 6 (colour online). Variation in temperature via viscosity ratio parameter β when We $= 0.6$, Br $= 0.3$, $x = 0.0$, $a_2 = 0.4$, $b_2 = 0.3$, $\gamma = \pi/4$, $d = 0.7$, $\eta = 0.7$, Pr $= 0.5$, $N_t = 0.5$, $N_b = 0.5$, and $a = 2.0$.

4. Graphical Analysis

In this section the graphical analysis of the numerical results has been carried out. Plots for axial velocity, temperature, and concentration profiles are presented and studied. Numerical values of heat and mass transfer rate at the boundary are presented in Tables 1 and 2. Effects of various quantities on the shear thickening and shear thinning fluids are separately analyzed in parts a and b of each Figure, respectively.

Examination of Axial Velocity

Effects of We, a, and β on the axial velocity are analyzed through Figures 1 – 3. All these figures depict that the velocity traces a parabolic trajectory with the maximum value occurring near the center of the channel. Two separate cases for $n > 1$ (shear thickening) and $n < 1$ (shear thinning) are studied. Figure 1a depicts that an increase in We results in an increase of the maximum value of velocity for $n = 2.5$ whereas the opposite behaviour is seen for $n = 0.5$. This highlights the fact that for a shear thickening fluid an increase in Weissenberg number yields an increasing effect on the velocity but for a shear thinning fluid its effect is reverse. The increase in non-Newtonian parameter a and viscosity ratio parameter β have the same effect on velocity in both cases. The maximum value of velocity is seen to decrease by increasing in a and β for a shear thickening fluid. Large values of a and β in the shear

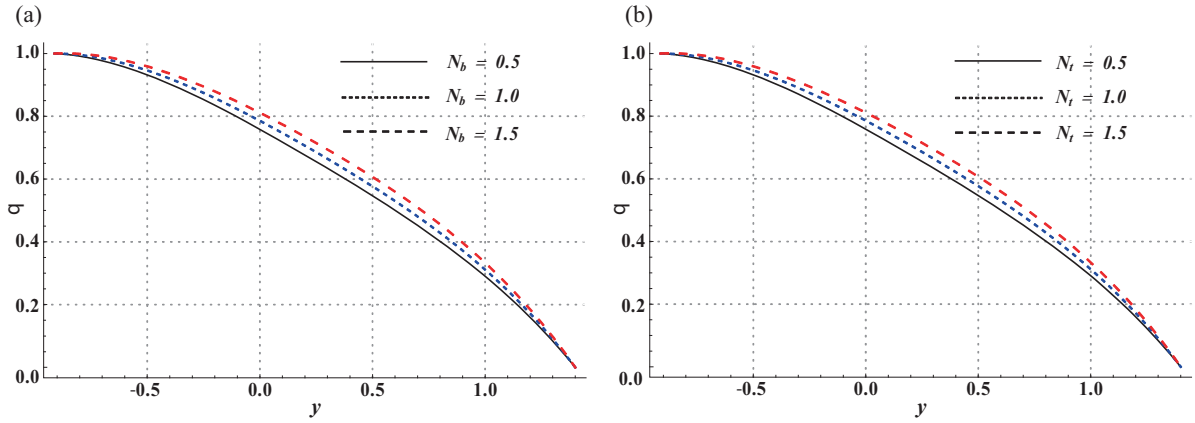

Fig. 7 (colour online). Variation in temperature via thermophoresis parameter N_t and Brownian motion parameter N_b when We $= 0.6$, Br $= 0.3$, $x = 0.0$, $a_2 = 0.4$, $b_2 = 0.3$, $\gamma = \pi/4$, $d = 0.7$, $\eta = 0.7$, Pr $= 0.5$, $a = 2.0$, and $\beta = 0.1$.

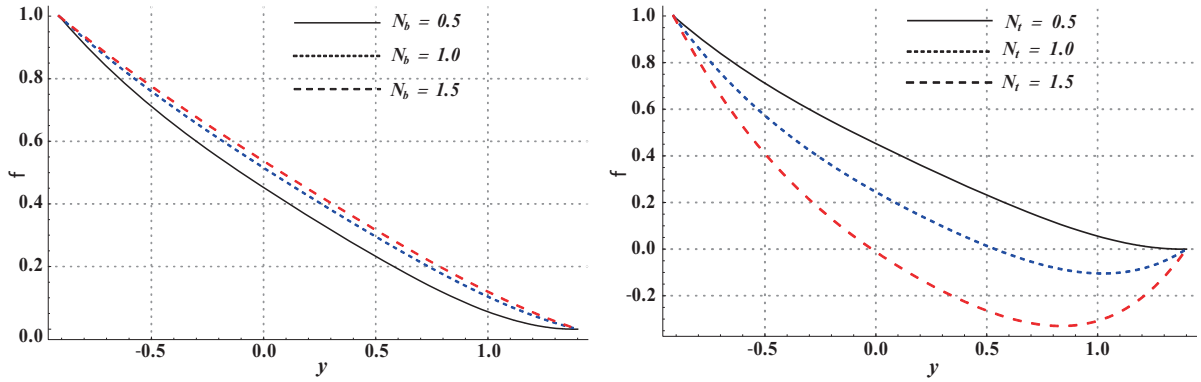

Fig. 8 (colour online). Development of concentration profile via thermophoresis parameter N_t and Brownian motion parameter N_b when We = 0.6, Br = 0.3, $x = 0.0$, $a = 0.4$, $\gamma = \pi/4$, $d = 0.7$, $\eta = 0.7$, Pr = 0.5, $a = 0.2$, and $\beta = 0.1$.

thinning fluid show an increase in the maximum value of velocity (see Figs. 2 and 3).

Variation in Temperature

The development of temperature profile is examined via Figures 4 – 7. The effects of different parameters on the shear thickening/thinning fluids are examined through these figures. An increase in We for the shear thickening case enhances the temperature. However temperature decreases when a and β are increased. On the other hand for a shear thinning fluid the temperature increases when there is an increase in a and β. A decrease in temperature is noticed when We increases. Figures 7a and b are plotted to examine the effect of the Brownian motion parameter N_b and thermophoresis parameter N_t on the temperature. These figures depict that the dimensionless temperature increases through large N_b and N_t.

Variation in Concentration

Figures 8 – 11 examine the effect of various parameters on the concentration of nanoparticles. The concentration increases through a larger Brownian motion parameter (see Fig. 8a). This is mainly due to the fact that an increase in N_b denotes the increase in haphazard motion of the nanoparticles which forbids them to settle at one place in the flow regime and consequently the concentration increases throughout the fluid. Figure 8b shows that the thermophore-

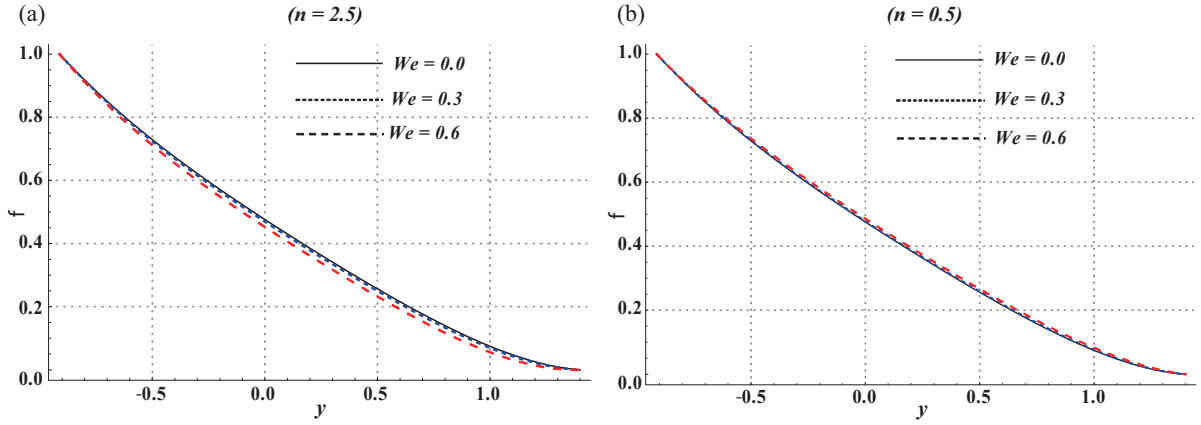

Fig. 9 (colour online). Development of concentration profile via Weissenberg number We when $a = 2.0$, Br = 0.3, $x = 0.0$, $a_2 = 0.4$, $b_2 = 0.3$, $\gamma = \pi/4$, $d = 0.7$, $\eta = 0.7$, Pr = 0.5, $N_t = 0.5$, $N_b = 0.5$, and $\beta = 0.1$.

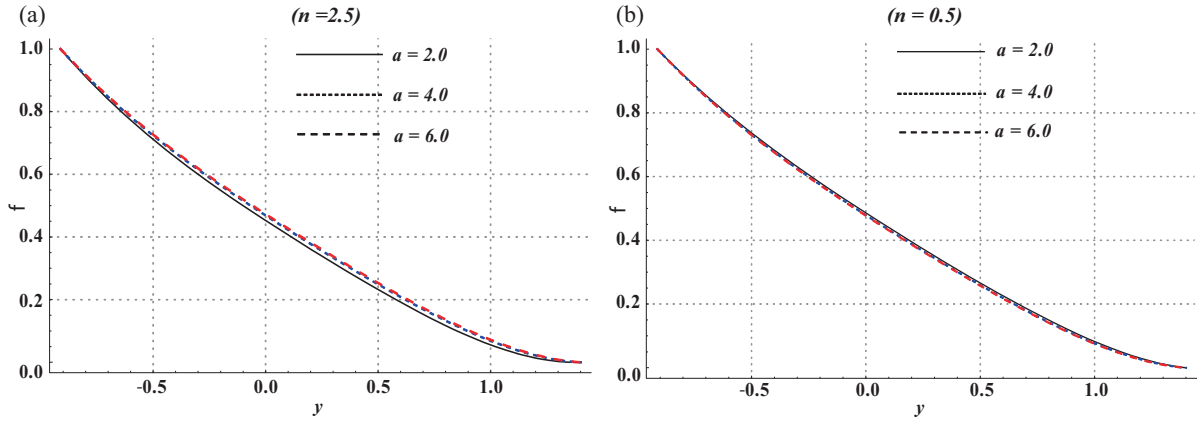

Fig. 10 (colour online). Development of concentration profile via non-Newtonian parameter a when We $= 0.6$, Br $= 0.3$, $x = 0.0$, $a_2 = 0.4$, $b_2 = 0.3$,$\gamma = \pi/4$, $d = 0.7$, $\eta = 0.7$, Pr $= 0.5$, $N_t = 0.5$, $N_b = 0.5$, and $\beta = 0.1$.

sis parameter has a decreasing effect on the concentration of nanoparticles. For the case of shear thinning fluid, the Weissenberg number We has an increasing behaviour whereas a and β have a decreasing effect on concentration. The concentration of nanoparticles immersed in a shear thickening fluid decrease when the Weissenberg number increases. However such concentration enhances for an increase in a and β.

Temperature and Concentration Transfer Rates

Numerical values of temperature and concentration rates at the upper wall are computed for a shear thickening fluid in Table 1 and for a shear thinning fluid in Table 2. For $n = 2.5$ the rate of heat transfer at the wall increases with an increase in We, N_t, and N_b whereas it decreases for a and β. Such increase is larger for N_b and N_t. The concentration transfer rate at the boundary for a shear thickening fluid decreases with an increase in We and N_t but it increases for a, β, and N_b. For $n = 0.5$, i. e. for the case of shear thinning fluid, We, a, and β have an opposite effect on heat and mass transfer rates when compared to the case for $n > 1$. However the effect of Brownian motion and thermophoresis parameter remain similar in both cases.

Tables 3 and 4 have been prepared to provide a comparison of present analysis with previous studies. A comparative study of present analysis with the

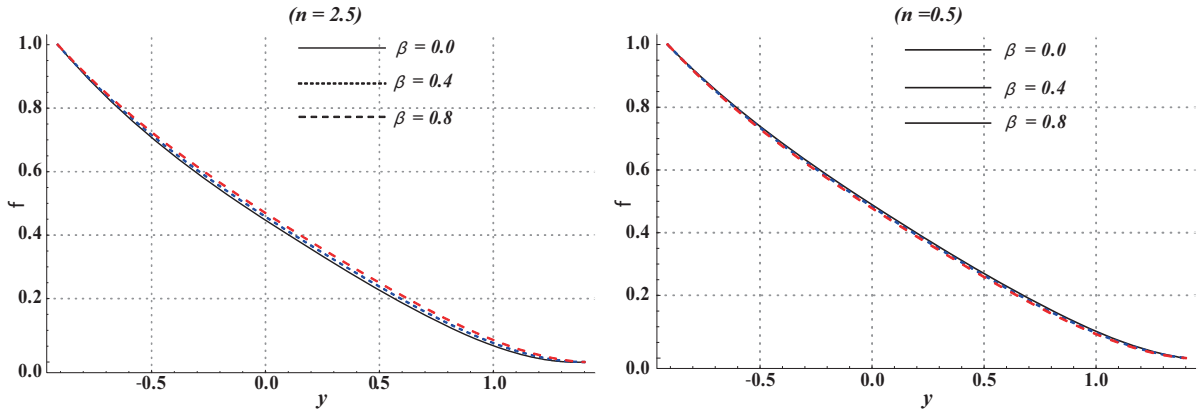

Fig. 11 (colour online). Development of concentration profile via viscosity ratio parameter β when We $= 0.6$, Br $= 0.3$, $x = 0.0$, $a_2 = 0.4$, $B_2 = 0.3$, $\gamma = \pi/4$, $d = 0.7$, $\eta = 0.7$, Pr $= 0.5$, $N_t = 0.5$, $N_b = 0.5$, and $a = 2.0$.

Table 1. Heat and mass transfer rates at the upper wall for shear thickening fluid ($n = 2.5$) when Br $= 0.3$, $x = 0.0$, $a_2 = 0.4$, $b_2 = 0.3$, $\gamma = \pi/4$, $d = 0.7$, $\eta = 0.7$, and Pr $= 0.5$.

We	a	β	N_t	N_b	$-\theta'(h_1)$	$-\phi'(h_1)$
0.0	2.0	0.2	0.5	0.5	0.812819	0.0521835
0.1					0.814893	0.0501098
0.2					0.821013	0.0439896
0.3					0.830939	0.0340636
0.05	1.0				0.810257	0.0547451
	2.0				0.813339	0.0516633
	3.0				0.812820	0.0521823
	4.0				0.812820	0.0521825
0.6	2.0	0.0			0.897176	−0.0321739
		0.1			0.889200	−0.0241972
		0.2			0.881162	−0.0161594
		0.3			0.873054	−0.0080512
		0.2	0.3		0.853033	0.1801820
			0.6		0.895486	−0.1230800
			0.9		0.939482	−0.4800640
			1.2		0.984986	−0.8934610
			0.5	0.3	0.853033	−0.2683860
				0.6	0.895486	0.0466807
				0.9	0.939482	0.1508450
				1.2	0.984986	0.2022990

previous attempts of Srinivas and Kothandapani [26] and Hayat et al. [20] is provided. Numerical results of the heat transfer coefficient at the upper wall ($Z = \theta_y(h_1)x$) through [26] is found in good agreement with the present study up to four decimal places (see Tab. 3). The heat transfer rate at the upper wall of present study is in good agreement with the results of Hayat et al. [20] (see Tab. 4). Present results also show that the axial velocity for both the Newtonian and Carreau–Yasuda fluid models trace a parabolic path with the maximum value near the center of the channel. The plot of axial velocity for a non-Newtonian fluid flattens near the center which is physically justified for a shear thinning fluid. Qualitatively all these results are in good agreement with the studies of Gijsen et al. [11, 12].

Table 2. Heat and mass transfer rates at the upper wall for shear thinning fluid ($n = 0.5$) when Br $= 0.3$, $x = 0.0$, $a_2 = 0.4$, $b_2 = 0.3$, $\gamma = \pi/4$, $d = 0.7$, $\eta = 0.7$, and Pr $= 0.5$.

We	a	β	N_t	N_b	$-\theta'(h_1)$	$-\phi'(h_1)$
0.0	2.0	0.2	0.5	0.5	0.812819	0.0521835
0.1					0.812124	0.0528788
0.2					0.810024	0.0549782
0.3					0.806477	0.0585254
0.05	1.0				0.81318	0.0518223
	2.0				0.812645	0.0523571
	3.0				0.812819	0.0521839
	4.0				0.812819	0.0521838
0.6	2.0	0.0			0.777285	0.0877179
		0.1			0.781687	0.0833154
		0.2			0.785671	0.0793317
		0.3			0.789429	0.0755736
		0.2	0.3		0.75867	0.2368
			0.6		0.799433	−0.0078162
			0.9		0.84175	−0.304146
			1.2		0.885588	−0.654907
			0.5	0.3	0.75867	−0.111113
				0.6	0.799433	0.126725
				0.9	0.84175	0.205141
				1.2	0.885588	0.243715

Table 3. Comparison of the numerical values of the heat transfer coefficient at the upper wall ($Z = \theta_y(h_1)x$) between the work of Srinivas and Kothandapani [26] and special case of present study when We $= 0.0$, $a_2 = 0.5$, $b_2 = 0.6$, $\gamma = \pi/4$, $d = 1.5$, $\rho = 0.5$, Pr $= 1.0$, $E = 3.0$, and $\beta = 0.0$ in absence of Brownian motion and thermophoresis effects.

x	Srinivas and Kothandapani [26]	Special case of present study
0.1	1.8449	1.84491
0.2	1.8352	1.83521
0.3	1.9738	1.97381

Table 4. Comparison of the numerical values of the heat transfer rate at the upper wall ($-\theta_y(h_1)$) between the work of Hayat et al. [20] and special case of present study when We $= 0.3$, $n = 0.5$, $a_2 = 0.4$, $b_2 = 0.3$, $\gamma = \pi/4$, $d = 0.7$, $\rho = 1.0$, Pr $= 1.0$, Br $= 0.3$, and $\beta = 0.0$, in absence of Brownian motion and thermophoresis effects.

x	Hayat et al. [20] for $M = 0$	Special case of present study
0.0	0.8091	0.80912
0.25	1.0081	1.00813
0.5	1.575	1.57501

5. Concluding Remarks

The peristaltic motion of a Carreau–Yasuda nanofluid in an asymmetric channel is studied. Main findings of present investigation are summarized below:

- The impact of the non-Newtonian parameters on flow quantities get reversed when we move from shear thinning to shear thickening fluids.
- The effect of Weissenberg number on velocity, temperature, and concentration is opposite to that of the other non-Newtonian parameters a and β.
- The Brownian motion and the thermophoresis parameter have an increasing effect on temperature.

- The concentration of the nanoparticles increases with an increase in the Brownian motion parameter but it decreases for an increase in the thermophoresis parameter.
- The heat transfer rate at the wall increases when N_b and N_t are increased.
- The mass transfer rate at the wall decreases by increasing N_t but increases with an increase in N_b.

Acknowledgements

We are thankful to the reviewers for the useful suggestions. This paper was funded by the Deanship of Scientific Research (DSR), King Abdulaziz University, Jeddah, under grant no. 26-130/1435 HiCi. The authors, therefore, acknowledge with thanks DSR for the technical and financial support.

[1] M. M. Rashidi, O. Anwar Bég, M. Asadi, and M. T. Rastegari, Int. J. Thermal Env. Eng. **4**, 13 (2012).
[2] M. M. Rashidi, N. Freidoonimehr, A. Hosseini, O. Anwar Bég, and T.-K. Hung, Meccanica **49**, 469 (2014).
[3] M. Mustafa, T. Hayat, I. Pop, S. Asghar, and S. Obaidat, Int. J. Heat Mass Transf. **54**, 5588 (2011).
[4] M. Sheikholeslami, M. Hatmi, and D. D. Ganji, Powder Technol. **246**, 327 (2013).
[5] M. Mustafa, S. Hina, T. Hayat, and A. Alsaedi, Int. J. Heat Mass Transf. **55**, 4871 (2012).
[6] M. Turkyilmazoglu, Chem. Eng. Sci. **84**, 182 (2012).
[7] M. Turkyilmazoglu, J. Heat Transf. Trans. ASME **136**, 31704 (2013).
[8] M. Turkyilmazoglu and I. Pop, Int. J. Heat Mass Transf. **59**, 167 (2013).
[9] T. Hayat, F. M. Abbasi, M. Al-Yami, and S. Monaquel, J. Mol. Liq. **194**, 93 (2014).
[10] M. Sheikholeslami and D. D. Ganji, Powder Technol. **235**, 873 (2013).
[11] F. J. H. Gijsen, F. N. van de Vosse, and J. D. Janssen, J. Biomech. **32**, 601 (1999).
[12] F. J. H. Gijsen, E. Allanic, F. N. van de Vosse, and J. D. Janssen, J. Biomech. **32**, 705 (1999).
[13] L. C. F. Andrade, J. A. Petronílio, C. E. de A. Maneschy, and D. O. de A. Cruz, J. Braz. Soc. Mech. Sci. Eng. **29**, 162 (2007).
[14] T. Hayat and F. M. Abbasi, Int. J. Numer. Methods Fluids **67**, 1500 (2011).
[15] T. Hayat, F. M. Abbasi, and A. A. Hendi, Chin. Phys. Lett. **28**, 44701 (2011).
[16] D. Tripathi, Int. J. Therm. Sci. **51**, 91 (2012).
[17] T. Hayat, F. M. Abbasi, and S. Obaidat, Magnetohydrodynamics **47**, 295 (2011).
[18] F. M. Abbasi, T. Hayat, A. Alsaedi, and B. Ahmed, Appl. Math. Inf. Sci. **8**, 211 (2014).
[19] F. M. Abbasi, T. Hayat, and B. Ahmad, J. Cent. South Univ. **21**, 1411 (2014).
[20] T. Hayat, F. M. Abbasi, A. Alsaedi, and F. Alsaadi, Z. Naturforsch. **69a**, 43 (2014).
[21] N. Ali, M. Sajid, T. Javed, and Z. Abbas, Int. J. Heat Mass Transf. **53**, 3319 (2010).
[22] Kh. S. Mekheimer, S. Z. A. Husseny, and Y. Abd Elmaboud, Numer. Meth. Partial Diff. Eqn. **26**, 747 (2010).
[23] Kh. S. Mekheimer, S. R. Komy, and S. I. Abdelsalamd, Chin. Phys. B **22**, 124702 (2013).
[24] S. Nadeem and N. S. Akbar, Z. Naturforsch. **68a**, 433 (2013).
[25] S. Nadeem, N. S. Akbar, and T. Hayat, Z. Naturforsch. **65a**, 901 (2010).
[26] S. Srinivas and M. Kothandapani, Int. Commun. Heat Mass Transf. **35**, 514 (2008).